Master's Thesis
석사 학위논문

Fabrication of Seebeck coefficient measurement system and thermoelectric properties in $Sn_{1-x}Ag_xTe$ compounds

Cho, Hyunyong(조 현 용 趙 顯 容)

Department of Emerging Materials Science
신물질 과학전공

DGIST

2015

Master's Thesis
석사 학위논문

Fabrication of Seebeck coefficient measurement system and thermoelectric properties in $Sn_{1-x}Ag_xTe$ compounds

Cho, Hyunyong(조 현 용 趙 顯 容)

Department of Emerging Materials Science
신물질 과학전공

DGIST

2015

Fabrication of Seebeck coefficient measurement system and thermoelectric properties in $Sn_{1-x}Ag_xTe$ compounds

Advisor : Professor Kwon, Yong Seung

Co-advisor : Professor Kim, Dong Hwan

by

Cho, Hyunyong

Department of Emerging Materials Science

DGIST

A thesis submitted to the faculty of DGIST in partial fulfillment of the requirements for the degree of Master of Science. The study was conducted in accordance with Code of Research Ethics[1]

12. 03. 2014

Approved by

Professor Kwon, Yong Seung _____

(Advisor)

Professor Kim, Dong Hwan _____

(Co-Advisor)

[1] Declaration of Ethical Conduct in Research**:** I, as a graduate student of KAIST, hereby declare that I have not committed any acts that may damage the credibility of my research. These include, but are not limited to: falsification, thesis written by someone else, distortion of research findings or plagiarism. I affirm that my thesis contains honest conclusions based on my own careful research under the guidance of my thesis advisor.

Fabrication of Seebeck coefficient measurement system and thermoelectric properties in $Sn_{1-x}Ag_xTe$ compounds

Cho, Hyunyong

Accepted in partial fulfillment of the requirements for the degree of Master of Science

12. 03. 2014

Head of Committee _____ (인)

Prof. Kwon, Yong Seung

Committee Member _____ (인)

Prof. Kim, Dong Hwan

Committee Member _____ (인)

Prof. Cho, Chang-Hee

MS/EM
201321014

조 현 용. Hyunyong Cho. Fabrication of Seebeck coefficient measurement system and thermoelectric properties in Sn1-xAgxTe compounds. Department of Emerging Materials Science. 2014. 35p. Advisors Prof. Kwon, Yong Seung, Prof. Co-Advisors Kim, Dong Hwan.

ABSTRACT

Pb-based materials, which are superior for thermoelectric performance, environmentally have toxicity. Thus the materials should be alternated by non-toxic materials.

Tin telluride (SnTe) is isostructural with PbTe and PbSe which are rock salt structure. In addition, SnTe is similar to the electronic band structure (two valence band system) with PbTe and PbSe. Thus, SnTe, which is overcome by low Seebeck coefficient and by large thermal conductivity, can be expected by good thermoelectric material. Thus, Ag-included poly crystals $Sn_{1-x}Ag_xTe$ (x=0.1, 0.2, 0.3, and 0.4) were prepared by box furnace and by hot press to confirm thermoelectric performance of the samples. By accident, we noticed difference that XRD patterns of $Sn_{1-x}Ag_xTe$ are changed from two phases (SnTe, AgTe) to mixed phase (SnTe/AgTe) before hot pressing and after. In addition, electrical conductivity of samples is maintained until high temperature. The power factor of sample to include silver(x=0.1) has maximum value (1.1

mW/mK^2) at 673K. However, SnTe has higher power factor than Ag-included SnTe. Nevertheless, we can carefully expect that sample to include mixed phase obtain high electrical conductivity.

Exceptionally, we developed the measurement of the thermoelectric power in the temperature range from 2K to 300K. By using two heaters, two thermometer, chip resistors, et al, measurement equipment is fabricated exactly. In addition, high density data is obtained by two heaters that are operated by turn. The system is controlled by LabVIEW software. In order to demonstrate this system, reference data of Pt wire and $Ca_{10}Na_x(Pt_3As_8)(Fe_2As_2)_5$ superconductor were calibrated by developed equipment. Therefore we demonstrated the equipment with superior performance through confirming calculated data.

Keywords: SnTe, mixed phase, electrical conductivity, Seebeck coefficient, power factor

Contents

List of Figure

List of Table

Chapter 1. INTRODUCTION

1. Thermoelectric effect

Fossil resources are being exhausted by the global energy consumption increase every year. Such a condition require the development and the use of alternative the energy sources. The thermoelectricity phenomenon is to convert directly thermal energy to electrical energy and vice versa. The phenomenon is used in power generation from waste heat or in the refrigeration by electric current. [1] This process is based on the Seebeck effect, which by a temperature gradient is generated as voltage difference in a material. Seebeck found that the needle of compass is deflected in the presence of dissimilar metals that are connected and are exposed to a temperature difference.

Thermoelectric element has a carrier of the n type and p type. The major carrier of n type and p type is electron and hole. As shown in Fig. 1.1 (a), p-n junctions at the top is heated by the heat source. Then, in this process, each carrier by temperature difference is transferred at cold site by heat and Electron hole pairs are recombined to generate power.

The inverse effect of Seebeck voltage, the occurrence of a temperature gradient by applied voltage, is known as the Peltier effect. As shown Fig. 1.1 (b), if voltage is applied in the right direction across a p-n junction, each carrier by applied voltage is transferred at the bottom. Thus, the device at the top can be cooled by applied voltage. [2, 3]

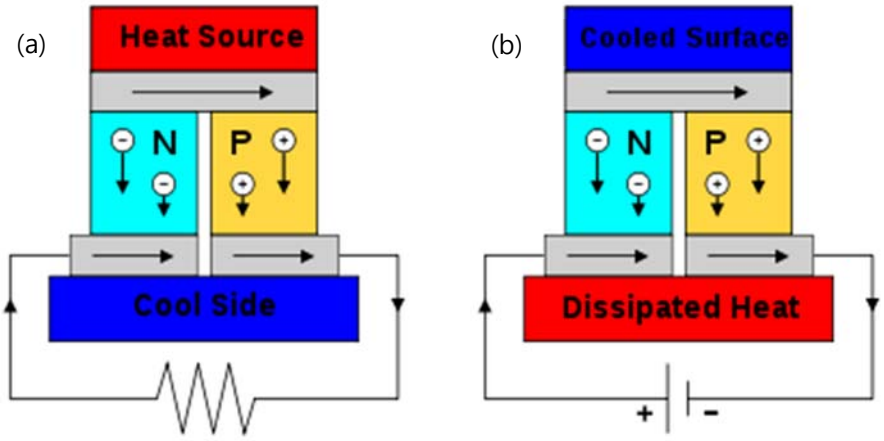

Figure 1.1 (a) Seebeck effect, (b) Peltier effect

2. Figure of merit (ZT) & Efficiency

Thermoelectric devices can be used for power generation as well as for refrigeration. Thermoelectric efficiency depends on Seebeck coefficient (S), electrical conductivity(σ), and thermal conductivity(κ). Figure of merit (ZT) by the three elements can be described as thermoelectric performance and is expressed as dimensionless,

$$\mathrm{ZT} = \frac{S^2\sigma}{\kappa}T \qquad \text{(Eq. 1.1)}$$

Where *T* is the absolute temperature.

Thermoelectric device performance relies directly on the temperature gradient and as intrinsic material parameter, the thermoelectric figure of merit. Thermoelectric device performance depends directly on the temperature gradient and on the thermoelectric figure of merit. The maximum efficiency of thermoelectric generation device is defined by combining the Carnot efficiency and the figure of merit as shown in (Eq. 1.2)

$$\eta_{max} = \frac{\Delta T}{T_H}\frac{\sqrt{1+ZT_{avg}}-1}{\sqrt{1+ZT_{avg}}+\frac{T_C}{T_H}} \qquad \text{(Eq. 1.2)}$$

Where T_H and T_C are the temperature of the hot and cold ends in devices, ΔT is their difference, $\Delta T/T_H$ is Carnot efficiency, and T_{avg} is the average temperature.

In this equation, the efficiency is significantly affected by figure of merit. In other words, high efficiency requires high figure of merit and large temperature difference in (Eq. 1.2). The correlation between the figure of merit and the efficiency of the thermoelectric device is shown in Fig. 1.2 [4].

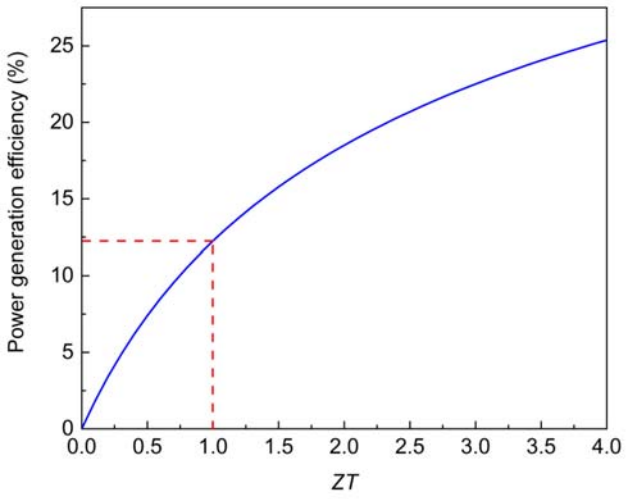

Figure 1.2 plot of power generation efficiency with the figure of merit ZT. [4]

In order to increase ZT values, the Seebeck coefficient and electrical conductivity should have a large value.

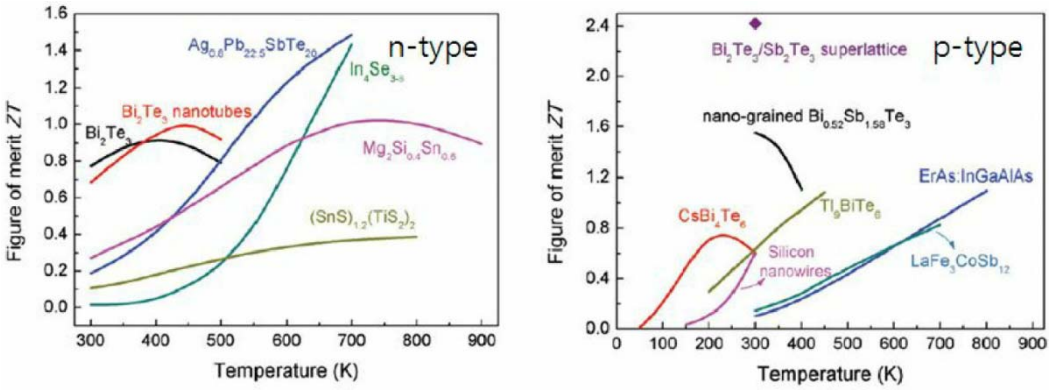

Figure 1.3 Thermoelectric figure of merit based on material

The ZT values of the current state of the art thermoelectric materials are shown in Fig. 1.3. The low-dimensional material is used to increase figure of merit ZT . Until 1990s, The Figure of merit was hovering at about 1, but the Figure of merit recently has been developed as Figure 1.3.

3. Carrier concentration

The figure of merit ZT depends on carrier concentration. In semiconductors there is a certain optimum carrier concentration. Because of low carrier concentration, insulators and non-degenerate semiconductor have large Seebeck coefficient. The carrier concentration correlates with Seebeck coefficient. The Seebeck coefficient of metals and degenerate semiconductors is expressed by:

$$S = \frac{8\pi^2 k_B^2}{3eh^2} m^* T \left(\frac{\pi}{3n}\right)^{2/3} \qquad \text{(Eq. 1.3)}$$

The large Seebeck coefficient requires Small carrier concentration (n) and large effective mass of carrier (m^*). In addition, the electrical conductivity which is affected to figure of merit is related to carrier concentration as following (Eq. 1.4)

$$\sigma = n\, e\, \mu \qquad \text{(Eq. 1.4)}$$

The thermal conductivity (Eq. 1.5) is composed of thermal conductivity of phonon and electron or hole. Besides, the thermal conductivity deals with carrier concentration by electron or hole. (Eq. 1.6)

$$\kappa = \kappa_e + \kappa_l \qquad \text{(Eq. 1.5)}$$

$$\kappa = L\sigma T = Lne\mu T \qquad \text{(Eq. 1.6)}$$

where L is the Loresz number with the value $2.45 \times 10^{-8} W\Omega K^{-2}$.

The Seebeck coefficient, electrical conductivity, and thermal conductivity correlate

strongly with carrier concentration as Figure 1.4.

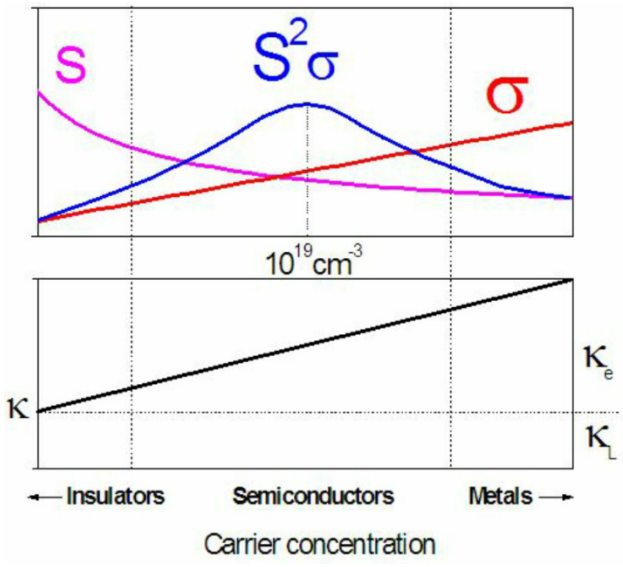

Figure 1.4 Correlation according to the carrier concentration with the Seebeck coefficient, electrical conductivity and thermal conductivity

Where $S^2\sigma$ is power factor which is important term in figure-of-merit equation.

In order to have high ZT, the carriers concentration should be maintained between $10^{19}$and 10^{21} carrier$/cm^3$.

4. $Sn_{1-x}Ag_xTe$

Lead chalcogenides (PbTe, PbSe, PbS) and alloys have been known to the thermoelectric materials with high performance. The p-type materials $Pb_{1-x}Na_xTe$-SrTe were reported with ZT value reaching ~2.2 about 915K. [5] In addition, thermoelectric performance of PbS and PbSe was reported with each ZT values 1.6 and 1.3.[6,7]

However, Pb-based materials environmentally have toxicity, thus the materials should be alternated by non-toxic materials.

Tin telluride (SnTe) is isostructural with PbTe and PbSe which are rock salt structure.

In addition, SnTe is similar to the electronic band structure with PbTe and PbSe.[8-13] Thus, SeTe can be expected by good thermoelectric material. However, because of many Sn vacancies, SnTe has high hole-density (p$\sim 10^{20} - 10^{21}\ cm^{-3}$). For this reason, SnTe has low Seebeck coefficient and large thermal conductivity. Nonetheless, several studies have demonstrated to have similar two valence band (light-hole and heavy-hole bands) in electronic band structures of PbTe, PbSe and SnTe.

SnTe has large energy difference to between two valence band edge about 0.3-0.4 eV [7, 9], and PbSe has energy difference (about 0.1 eV [14]) in less than SnTe. (Figure 1.5 [23])

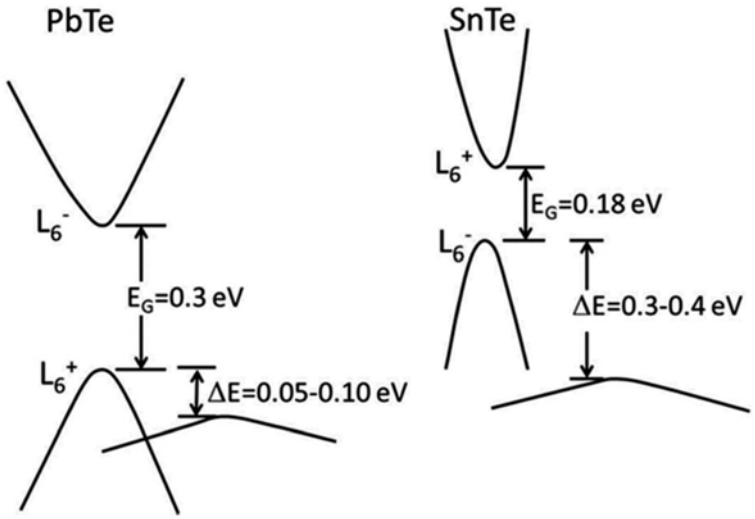

Figure 1.5 a schematic diagram of the near edge band structure in PbTe and SnTe

In SnTe, Seebeck coefficient has the varied value about carrier concentration by Seebeck Pisarenko relation. Here, Figure 1.6 [23] is Pisarenko plot, and Seebeck coefficient is observed with the carrier concentration.

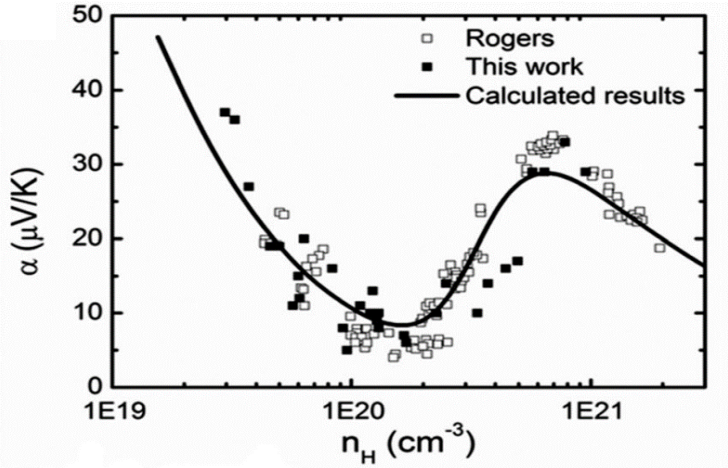

Figure 1.6 Seebeck coefficients with carrier concentration.

Recently, In-doped and Cd-doped SnTe is reported with ZT value 1.1 at 873K and with ZT value 1.3. [15, 16]

Also, the layered chalcogenides (MoS_2, $MoSe_2$, $MoTe_2$) were reported with enhancement of thermoelectric power factor by layer mixing. [17] The enhanced power factor is caused by reducing the band gap that has electrical conductivity because of layer mixing (See in Figure 1.7 [17])

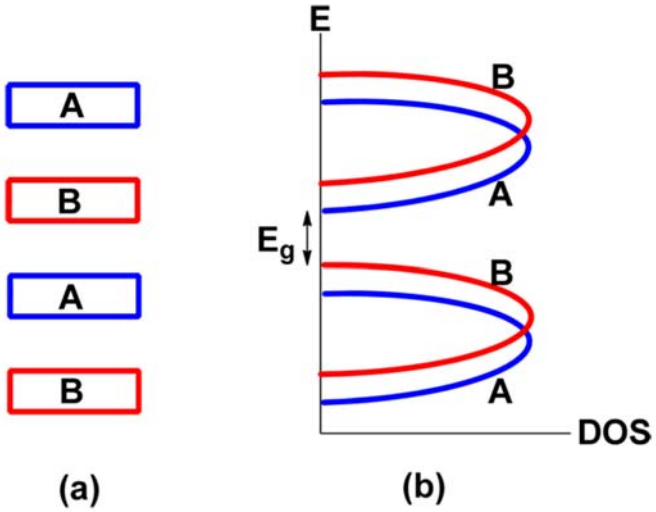

Figure 1.7 Reducing band gap by mixing layer (a) mixing of layers (b) band gap of a mixed layer system [17]

Where A and B are each layers. Figure 1.7 (b) shows reason why band gap is decreased at each valance band edge and conduction band edge.

In this study, we noticed difference of XRD patterns of $Sn_{1-x}Ag_xTe$ (x=0.1, 0.2, 0.3, and 0.4) before hot pressing and after. Before hot pressing, the samples separated into two phases with SnTe and AgTe. However, after hot pressing, AgTe peaks disappeared and SnTe peaks shifted to high angle. The sharp peaks changed broad peaks by hot pressing. In addition, Power factor of the samples was increased at low temperature region. Then, the reduction ratio of the electrical conductivity of $Sn_{1-x}Ag_xTe$ is lower than SnTe. Thus, electrical conductivity of the samples was roughly maintained until high temperature. Consequently, we suggest carefully that the mixed samples (SnTe/AgTe) change power factor at low temperature region and lattice parameter, like mixing layer system [17].

Chapter 2. Theory

1. Seebeck effect

When the temperature difference occurs within material, the electromotive force is generated in a material. Generated voltage is called thermo electromotive force. The temperature difference is proportional to the generated voltage at both ends. It can be expressed by the following Equation 2.1.

$$\mathrm{Vs} = \mathrm{aA} \cdot \Delta\mathrm{T} \qquad \text{(Eq. 2.1)}$$

In the equation, aA is the proportionality constant, is defined as for absolute Seebeck coefficient. If Seebeck coefficient of two conductors is aA and aB, Seebeck coefficient between two materials can be appeared as following Equations 2.2.

$$\mathrm{aA} - \mathrm{aB} = \frac{\mathrm{dVs}}{\mathrm{dT}} = \frac{dVB}{dT} - \frac{dVA}{dT} = aB - aA \qquad \text{(Eq. 2.2)}$$

Seebeck coefficient is indicated generally Equation 2.3.

$$\mathrm{S} = \frac{8\pi^2 k_B^2}{3eh^2} m^* T \left(\frac{\pi}{3n}\right)^{2/3} \qquad \text{(Eq. 2.3)}$$

Where n is carriers concentration, m* is effective mass of carriers. [18] Thus large Seebeck coefficient requires large effective mass and small carrier concentration about degenerate semiconductors and metal.

However, in the case of non-degenerate semiconductors, charged carriers need to be excited across the band gap Energy (E_g) to the conduction level. Thus, the Seebeck coefficient of semiconductors can be approximately expressed as following Equation 2.4.

$$\mathrm{S} \approx \left(\frac{k_B}{e}\right) \frac{E_g}{k_B T} = \frac{E_g}{eT} \qquad \text{(Eq. 2.4)}$$

Boltzman transport theory is described about transport with electron and heat.

This theory by Motto equation [19] (Eq. 2.5) is generally described about Seebeck coefficient.

$$S = \frac{\pi^2}{3}\frac{k_B^2 T}{e}\frac{dln\sigma(E)}{dE}\Big|_{E=E_F} \qquad \text{(Eq. 2.5)}$$

σ(E) is electrical conductivity to be decided by Fermi energy. If scattering of electrons has nothing to do with Energy, σ(E) is only proportional to density of state (DOS). Figure 2.1 shows about different two electronic DOS.

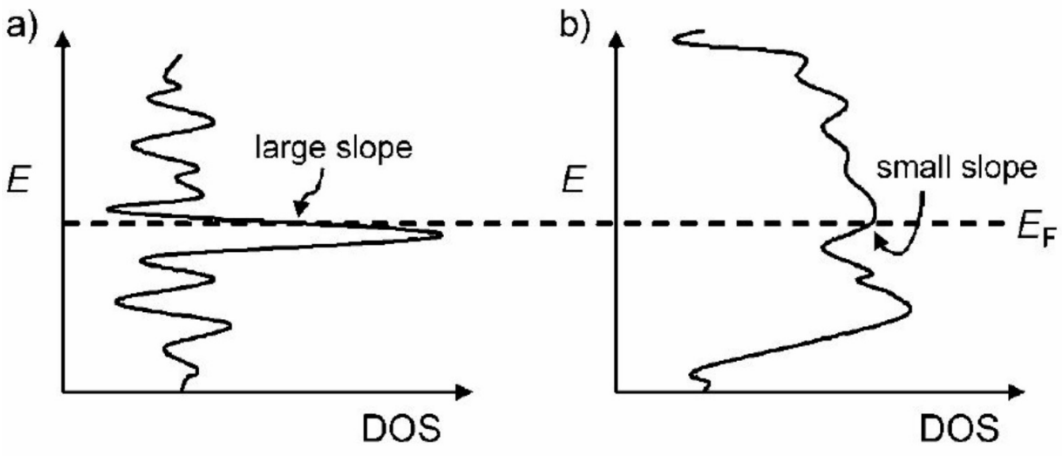

Figure 2.1 (a) $\frac{dln\sigma(E)}{dE}$ large slope, (b) small slope nearby Fermi energy.

Previously mentioned, Seebeck coefficient is associated with slope nearby Fermi energy by Motto equation. Thus large slope means large Seebeck coefficient and small slope signify low Seebeck coefficient.

2. Effects of charge carrier's interactions on Seebeck coefficients

Electron-electron interactions

The Seebeck coefficient is a fundamental electronic transport property. The Seebeck coefficient is influenced by interactions of charge carriers with one other.

The Seebeck coefficient is the entropy which is transported by charge carrier. The entropy is affected by the addition of a charge carrier and by the absolute temperature. Thus, the Seebeck coefficient is the sum of contributions by the presence charge carriers and their transport:

$$\alpha = \alpha_{presence} + \alpha_{transport} \qquad \text{(Eq. 2.6)}$$

In this chapter, because of confusing symbol of entropy, Symbol of the Seebeck coefficient is α

For example, consider the idealized situation in which n fermion charge carriers are distributed among N degenerate states of an arbitrarily narrow energy band. Then the entropy of distributing n fermion charge carriers among the N state is demonstrated as following equations:

$$S = k\ln\Omega = k\ln\frac{N!}{n!(N-n)!} \qquad \text{(Eq. 2.7)}$$

$$S = -k\left\{N\ln\left(1-\frac{n}{N}\right) - n\ln\left(\frac{N}{n}-1\right)\right\} \qquad \text{(Eq. 2.8)}$$

$$S = -Nk[c\ln c + (1-c)\ln(1-c)] \qquad \text{(Eq. 2.9)}$$

Where $c \equiv n/N$ is the carrier concentration. The Seebeck coefficient is related by adding a single carrier:

$$q\alpha = \frac{\partial S}{\partial n} = k\ln\left[\frac{1-c}{c}\right] \qquad \text{(Eq. 2.10)}$$

Then, this equation can be expressed about energy terms via the Fermi function, $c = 1/\exp[(E-\mu)/kT]+1$ as following equation.

$$\alpha = \frac{k}{q}\left[\frac{(E-\mu)}{kT}\right] \quad \text{(Eq. 2.11)}$$

Where μ is chemical potential, kT is the thermal energy.

However, each electron carriers have a magnetic moment. Thus, each electronic orbital state can be occupied both by carrier of spin up and by a carrier with spin down and two carrier can be filled in the orbital state. Here, filled orbital state should be considered by spin state of two electrons, because same spin electron is not filled in orbital state by Pauli's exclusion principle. A carrier can equivalently have one of two spin value, spin up or spin down in orbital. Thus, Seebeck coefficient is

$$\alpha = \frac{k}{q}\left[\frac{2(E-\mu)}{kT}\right] \quad \text{(Eq. 2.12)}$$

3. Thermal conductivity

Thermal conductivity coefficient (κ) of the solid is defined about flowing heat and expressed as following equation.

$$j_u = -\kappa \frac{dT}{dx} \qquad \text{(Eq. 2.13)}$$

Where j is flux which be defined as unit area per unit time passing through the energy of heat energy. The equation means that heat energy is transferred at random process. In other words, the flux experiences frequent clash in the material.

Because of random process of heat flux, equation of flux includes temperature gradient and mean free path.

Thermal conductivity coefficient is expressed as follows.

$$\kappa = \frac{1}{3} Cvl \qquad \text{(Eq. 2.14)}$$

Where C is heat capacity per unit volume, v is average speed of particles, l is mean free path of particles.

Particle flux is $n < |v_x| > /2$ and exist as the opposite direction of the same size. Where n is particle concentration. Specific heat of a particle is c. If a particle temperature change as ΔT, a particle release energy as cΔT. Then temperature gradient is expressed as follows.

$$\Delta T = \frac{dT}{dx} l_x = \frac{dT}{dx} v_x \tau \qquad \text{(Eq. 2.15)}$$

Where τ is average time between collisions. Next equation can be explained about the opposite direction flux.

$$j_u = -n < v_x^2 > c\tau \frac{dT}{dx} = -\frac{1}{3} n < v^2 > c\tau \frac{dT}{dx} = -\frac{1}{3} Cvl \frac{dT}{dx} \qquad \text{(Eq. 2.16)}$$

If the speed is constant, because of $l \equiv v\tau$ and $C \equiv nc$, thermal conductivity

coefficient become $Cvl/3$.

In a solid, there are two sources for thermal conductivity. When the carriers are electrons which are transferring heat, the carriers are provided as electronic contribution of thermal conductivity(κ_e). The other contribution to the thermal conductivity is the lattice thermal conductivity transported by lattice vibration (κ_l). Most of the electronic term is directly related to the electrical conductivity through the Wiedemann-Franz law,

$$\kappa = L\sigma T = Ln e \mu T \qquad \text{(Eq. 2.17)}$$

Where L is the Loresz number with the value $2.45 \times 10^{-8} W\Omega K^{-2}$.

Lattice vibrations can be described as atoms vibrating more energetically at on part of a solid transferring that energy to less energetic neighboring atoms and lattice vibration correlate with Phonon travelling. As a result, thermal conductivity is expressed by the equation.

$$\kappa = \kappa_e + \kappa_l \qquad \text{(Eq. 2.18)}$$

Chapter 3. Seebeck coefficient measuring equipment

In this chapter, we explain the development of an experimental setup for the thermoelectric power measurement (Seebeck coefficient) in OXFORD INSTRUMENTS, Cryogenic superconducting magnets equipment. Our equipment (Fig. 3.1) can be measured in the temperature range from 2 to 300K, and is composed of two heaters, two thermometers, chip resistors, etc. High density data with increasing temperature is obtained from equipment. In order to demonstrate the system, calibrations have been performed on a platinum wire and $Ca_{10}Na_x(Pt_3As_8)(Fe_2As_2)_5$ superconductors. All equipment (current sources, voltmeters, etc.) were controlled by LabVIEW software.

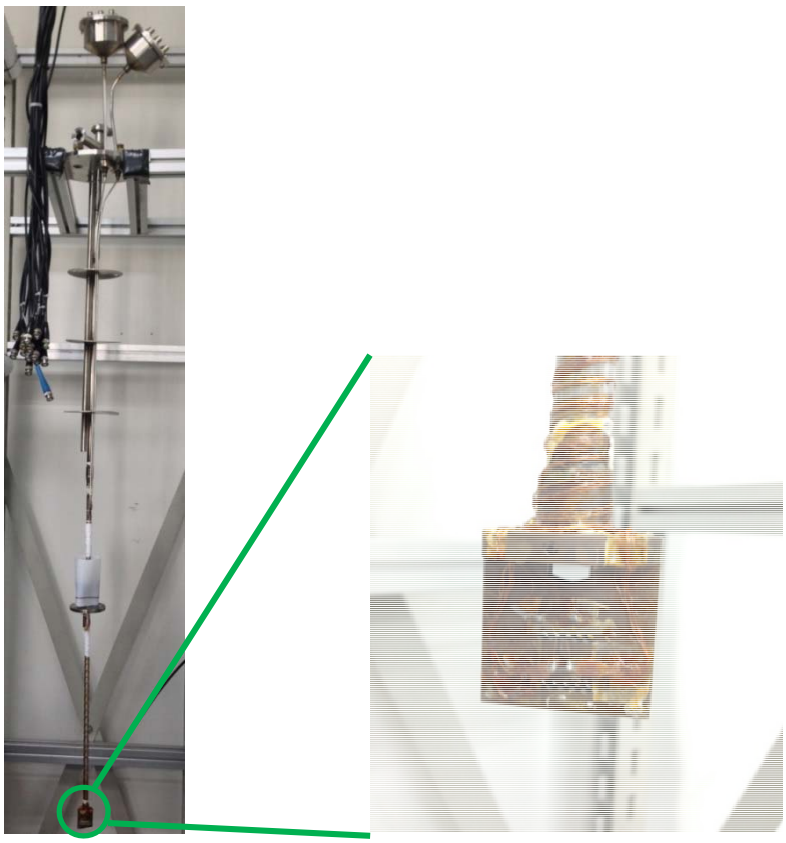

Figure 3.1 Photos of completed holder

1. Experimental setup

This equipment was produced to adapt cryostat system. Figure 3.2 show the sample stage on the heat sink. The sample stage was composed of high sensitive thermometers (Cernox sensors) at low temperature, heater (120Ω strain gauge), thermally isolated G-10 plate, chip resistors to raise the temperature, and phosphor bronze wire.

We will describe producing process of sample stage and experimental method. First, G-10 plate was glued to the bottom of the thermometer using the GE varnish. The distance between two stages has short length (~1.5mm) and long length (~2mm). Second, two heater using the GE varnish were attached on the thermometer. Finally, phosphor bronze wires which have low Seebeck coefficient (below 0.5μV K^{-1}) were fixed by using a silver epoxy on the two thermometers and chip resistor for increase of this system temperature was attached to opposite site of sample stage. In order to experiment the system, the sample roughly 2mm may be fixed using the silver paste in a complete holder. Then the sample measurement can be used by LabVIEW software.

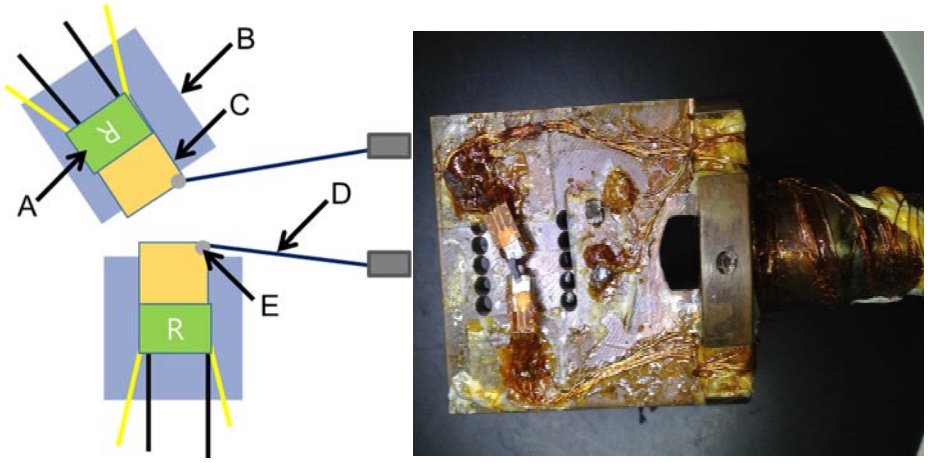

Figure 3.2 (a) Schematic diagram of sample stage. A: strain gauges for heater, B: G-10 plate for thermal isolation from the heat sink, C: thermometer, D: Phosphor bronze wire, E: silver epoxy for fixed Phosphor bronze wire on thermometers. (b) Sample settles on thermometers using the silver paste.

2. Operating principles

The sample holder is provided only 16 wires. Eight wires were used for two thermometers, four wires were used for the heater, two wires were used for the voltage difference, and two wires were used for chip resistor.

Current source is supplied as heat reservoir to heater. The heat provides temperature difference between two thermometers. Temperature difference serves voltage difference by carriers of sample and the difference is measured by voltmeter. By this time the Seebeck coefficient is calculated by voltage and temperature difference. Because two heaters were operated by turn, high density Seebeck coefficient data can be measured. The system is controlled by LabVIEW software.

When we apply a small temperature difference across the sample, we can define temperature and voltage about applied heat. T_i represents temperature just before turn on heaters and T_f indicates temperature just before turn on heaters. Therefore, by ΔV and ΔT the sample temperature and Seebeck coefficient are calculated as following equations:

$$2\Delta T = (T_{2f} - T_{1f}) + (T_{1i} - T_{2i}) \quad \text{(Eq. 3.1)}$$

$$2\Delta V = (V_f - V_i) \quad \text{(Eq. 3.2)}$$

$$T_{av} = \frac{(T_{2f}+T_{1f})+(T_{1i}+T_{2i})}{4} \quad \text{(Eq. 3.3)}$$

By temperature difference Seebeck coefficient of the sample is calculated by $S = 2\Delta V/2\Delta T$.

3. Calculation of sample Seebeck coefficient

In this chapter, we will describe that calibrations have been performed on Pt wire and $Ca_{10}Na_x(Pt_3As_8)(Fe_2As_2)_5$ superconductors. The system was compared with Pt reference data and resistivity data of superconductors.

Figure 3.3 shows Seebeck coefficient of Pt wire. The results of Pt wire match with reference data. The estimated uncertainty of this system from 77K to300 K temperature ranges falls within a maximum of ±1 μV K^{-1}.

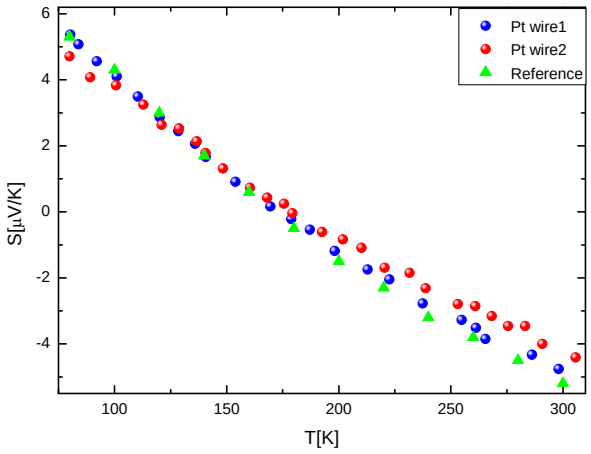

Figure 3.3 Seebeck data of Pt wire is compared with the reference data. Circles line represents the measured data and solid triangles data is reference from [20].

Because Seebeck coefficient and resistivity are zero in the superconducting state, the superconductor can be used by reference. Superconductor with a transition temperature of 37K degree was created in our lab. So we could compare Seebeck data with resistivity data.

The Seebeck data of sample correspond roughly to resistivity in superconducting transition temperature in Figure 3.4. Therefore, the equipment from room temperature to 4K was identified by calculated data.

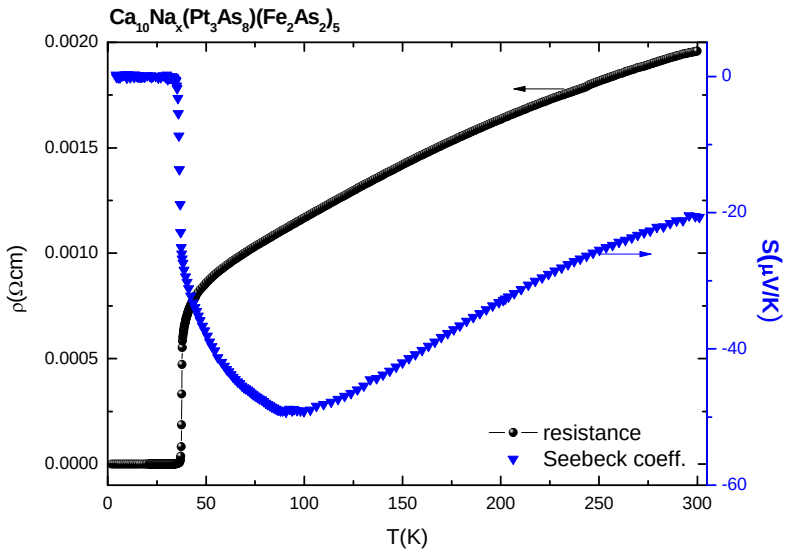

Figure 3.4 Seebeck coefficient (left axis) and electrical resistivity (right axis) data

Chapter 4. Thermoelectric property of $Sn_{1-x}Ag_xTe$

1. Experimental Methods

(1) Samples preparation

Ag-doped poly crystals $Sn_{1-x}Ag_xTe$ (x=0.1, 0.2, 0.3, and 0.4) were prepared by box furnace and by hot press. The samples were fabricated by using high purity (99.999%) elements Sn, Ag and Te to be calculated mole fraction. Prepared samples were loaded in and evacuated quartz tube under high vacuum (~10^{-6} torr) by using rotary pump and diffusion pump. Then, impurities (N_2, O_2, H_2O, etc.) were repeatedly purged by using the argon gas in quartz tube. Afterward quartz tube was sealed to make quartz ample. The elements were heated at 950℃ for 12 hour in box furnace (Figure 4.1. (a)). Then, the melted samples were cooled to 550℃ for 40 hour and the samples is cooled to room temperature without impacting around. The melted ingots were pulverized.

Figure 4.1 (a) Box furnace (b) Hot Press

The melted ingots were pulverized by hand milling. The powders were sintered at 580℃ by hot press (Figure 4.1(b)) under pressure of 70MPa for 1 hour. As a result the samples of Pellet form were obtained.

(2) Seebeck Coefficient, electrical conductivity measurement

In order to measure Seebeck coefficient and resistance, the samples with cylinder shape were produced as horizontal ~4mm, vertical ~4mm, and height ~9mm. The samples were measured by using four point probe method by using the equipment (ULVAC, ZEM3) from room temperature to 673K.

When the temperature difference occurs within a material, the electromotive force is generated in a material. The generated voltage is measured by the measurement, and Seebeck coefficient is calculated by difference temperature and voltage as following equation. Figure 4.2 is about equipment principle.

$$S = \frac{V\alpha}{\Delta T} \qquad \text{(Eq. 4.1)}$$

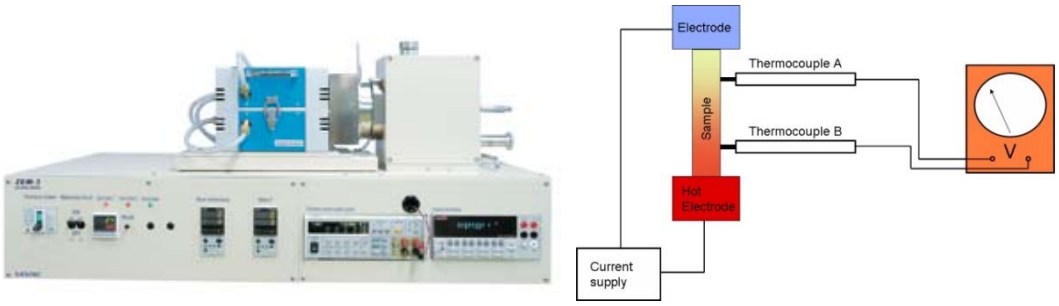

Figure 4.2 ULVAC, ZEM3, Seebeck coefficient, resistivity measurement equipment.

Where $V\alpha$ is electromotive force, ΔT is temperature difference.

Four-probe method was used to measure the electrical resistivity in experiment. Contact resistivity disappears by four probe method. Current is supplied as the outer two probes by a current source; voltmeter measures the voltage across the inner two probes. Thus resistivity is measured by method as following equation.

$$\rho = \frac{\Delta V}{I} \times \frac{A}{L} = \frac{V_\alpha A}{IL} \ [\Omega cm] \qquad \text{(Eq. 4.2)}$$

Where A is sample area, L is distance between the probe.

2. Results and Discussion

(1) X-Ray Diffraction

In order to characterize $Sn_{1-x}Ag_xTe$ (x=0.1, 0.2, 0.3, 0.4) of poly crystals, the samples is measured by x-ray powder diffraction before hot press and after. Figure 4.3 shows the x-ray diffraction (XRD) pattern for $Sn_{1-x}Ag_xTe$ on room temperature and that peak shifted across high angle with Ag-concentration. After hot pressing, AgTe peaks disappeared and SnTe peaks shifted to high angle. The sharp peaks were changed to broad peaks by hot pressing (see in inner Figure 4.3(b). Inner Figure 4.3 (b) show that peak positions after hot press shift between SnTe peak and AgTe peak.

SnTe that has NaCl type crystal structure was reported by reference [21]. In addition, Space group of tin telluride that has Cubic structure is Fm3m, such as AgTe [22].

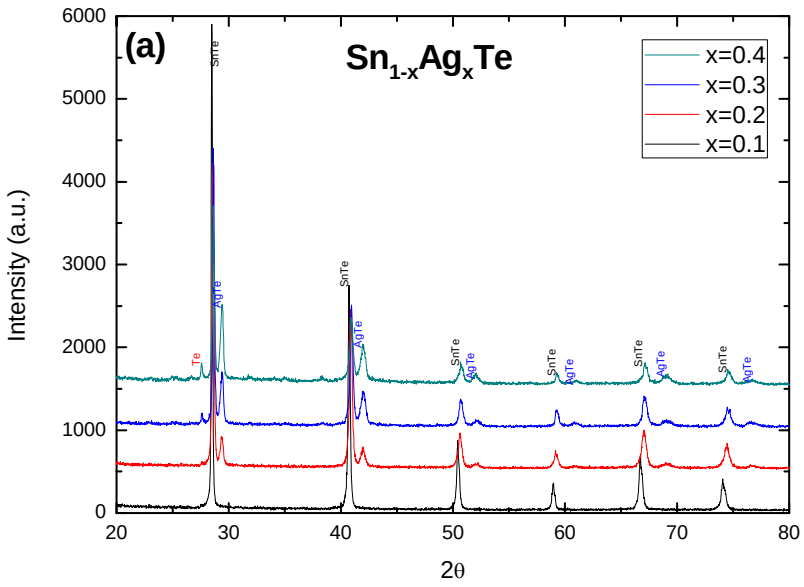

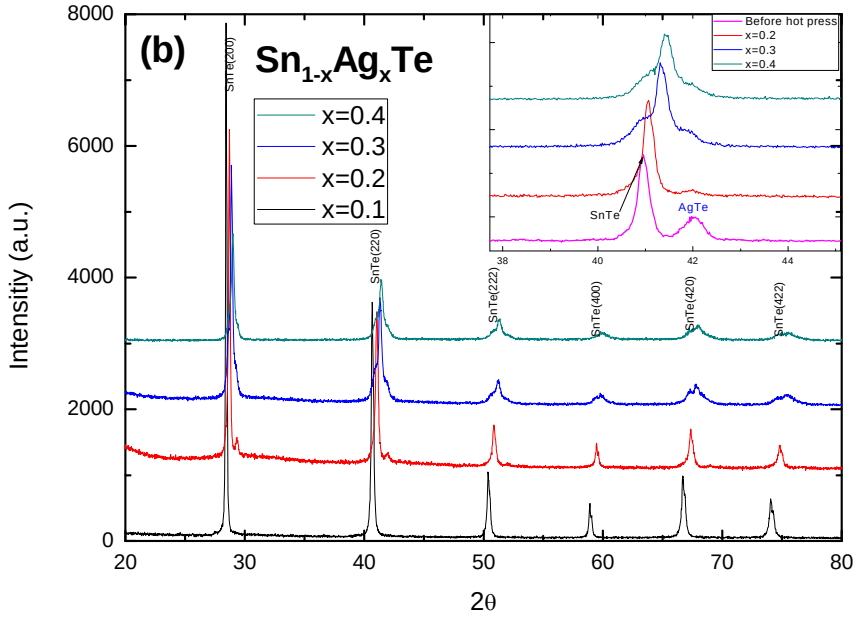

Figure 4.3 Powder XRD patterns of $Sn_{1-x}Ag_xTe$ for x=0.1, 0.2, 0.3, 0.4. (a) Before hot press XRD patterns (b) After hot press XRD patterns

As the analysis results, the lattice parameter of a-axis decreased with Ag-concentration in Figure 4.4.

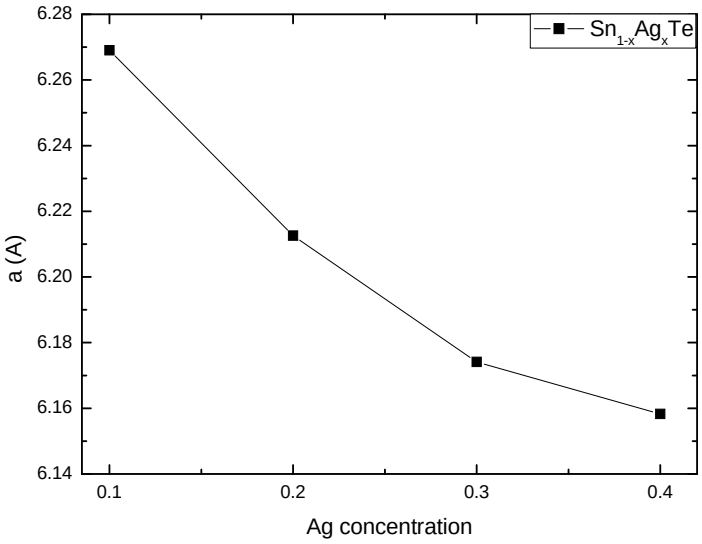

Figure 4.4 The lattice constants with Ag doping concentration

The lattice parameters (a) of samples with doping concentration has 6.2690 Å (x=0.1), 6.2126 Å (x=0.2), 6.1741 Å (x=0.3), 6.1583 Å (x=0.4). As a result, we suggest that SnTe and AgTe were mixed by hot pressing at grain boundary. As with the results of mixing layer system [17], with increasing Ag-concentration, the samples change lattice parameter by mixed SnTe/AgTe.

(2) Scanning electron microscopy and Energy Dispersive Spectroscopy

Scanning electron microscopy was used to confirm the image of the atomic surface and the atomic percentage of the single crystal. Scanning electron microscope (SEM) is incident into sample by the electron beam generated by the electron gun. At this time, a back-scattered electron or secondary electron is emitted. These detected electrons are observed and analyzed surface of the sample. Additionally, it is possible to examine the atomic percentage ratio using Energy dispersive spectroscopy (EDS).

In order to confirm atomic composition with Ag-concentration, $Sn_{1-x}Ag_xTe$ is measured by SEM and EDS in Figure 4.5 and Table 4.1. Figure 4.5 also shows the EDS result, and the data confirmed that the samples were composed by Sn, Ag, and Te. In addition, Table 4.1 indicates atomic composition ratio. However, we noticed that Sample was fabricated less than amount of planned Ag-concentration. Nevertheless, Ag concentration of the samples increased in sample with Ag-concentration.

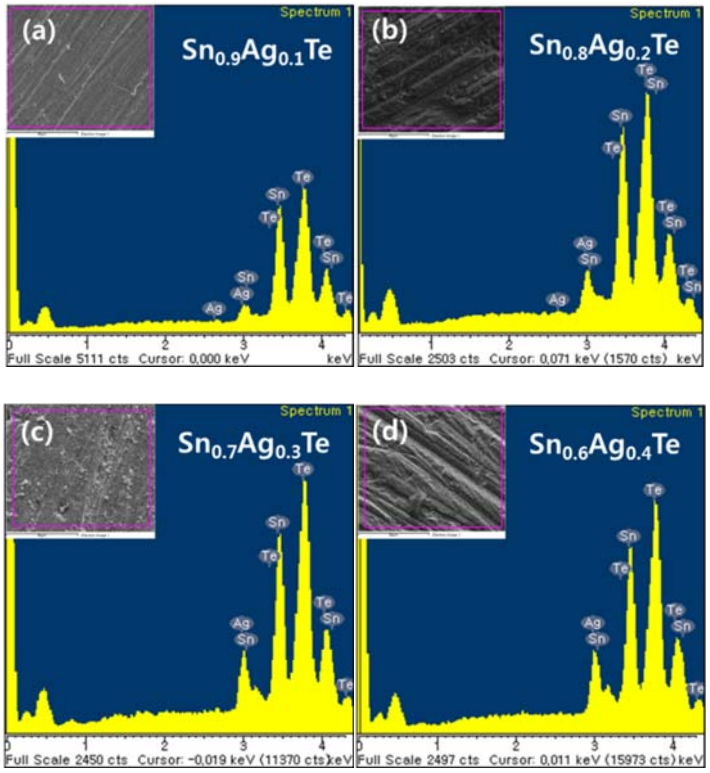

Figure 4.5 SEM image and EDS results With Ag concentration

at% (Te reference ratio)	Sn	Ag	Te
$Sn_{0.9}Ag_{0.1}Te$	46.08(0.9368)	4.73(0.0961)	49.19(1)
$Sn_{0.8}Ag_{0.2}Te$	44.77(0.9384)	7.53(0.1578)	47.71(1)
$Sn_{0.7}Ag_{0.3}Te$	40.84(0.8440)	10.78(0.2228)	48.39(1)
$Sn_{0.6}Ag_{0.4}Te$	39.8(0.8325)	12.39(0.2591)	47.81(1)

Table 4.1 Atomic composition ratio with Ag-concentration

(3) Seebeck coefficient

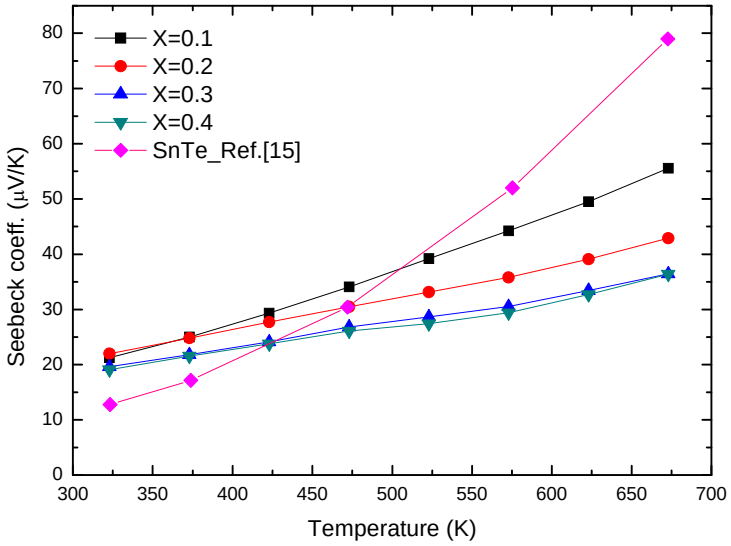

Figure 4.6 Temperature dependent Seebeck coefficient with Ag doping

Figure 4.6 shows Seebeck coefficient of $Sn_{1-x}Ag_xTe$. The Seebeck coefficient of each sample is positive value which means that dominant charge carrier is a hole. Overall, the Seebeck coefficient decreased with increasing Ag- concentration. SnTe [15] at low temperature had the low Seebeck coefficient. However, at high temperature, the Seebeck coefficient of $Sn_{1-x}Ag_xTe$ is lower than SnTe. Nonetheless, $Sn_{0.9}Ag_{0.1}Te$ compound shows high Seebeck coefficient of approximately 55 μV/K, at 673K. While the x=0.4 samples show low Seebeck coefficient of approximately 36 μV/K at 673K. Nonetheless, Seebeck coefficient of all samples is larger than reference sample.

(4) Electrical conductivity

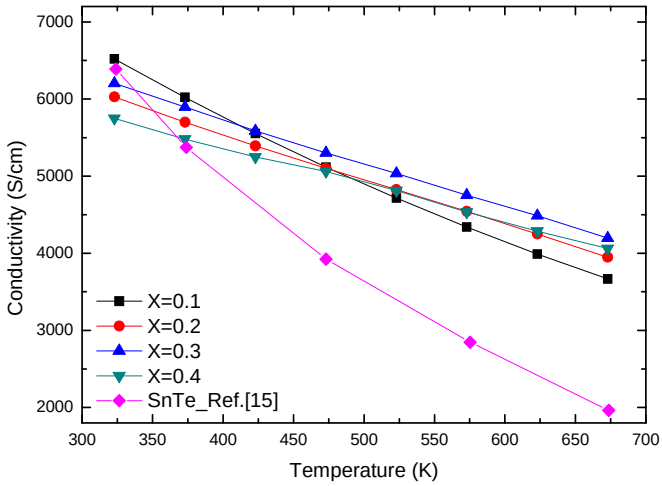

Figure 4.7 Temperature dependent electrical conductivity

Figure 4.7 shows electrical conductivity of $Sn_{1-x}Ag_xTe$. SnTe [15] at high temperature reported low electrical conductivity. However Ag-doped samples have larger electrical conductivity than SnTe at the high temperature. In addition, at low temperature region, $Sn_{1-x}Ag_xTe$ is pretty similar to SnTe. Overall, with temperature, decreasing rate of electrical conductivity of $Sn_{1-x}Ag_xTe$ is lower than SnTe. In other words, electrical conductivity of SnTe decreases rapidly with increasing temperature.

Similar to the results of mixing layer system [17], by doping and mixing (AgTe/SnTe), electrical conductivity of the samples is well-maintained until high temperature. Because of mixing phase (SnTe/AgTe) in grain boundary, the samples become more metallic than SnTe. Thus, at high temperature, the samples have larger electrical conductivity than SnTe.

(5) Power factor

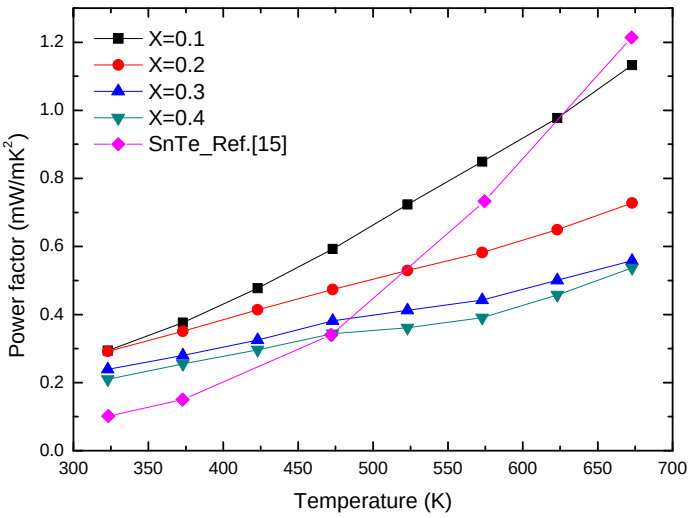

Figure 4.8 Temperature dependence of power factor from ~300K to ~700K

The power factors calculated from Seebeck coefficient and electrical conductivity with various temperatures. The power factor of SnTe is 1.2 mW/mK^2 at 673K, and SnTe has higher power factor than samples that contains Ag. In addition, with increasing Ag-concentration, the power factors decrease along with Seebeck coefficient of the samples. Then, power factor of SnTe is lower than $Sn_{1-x}Ag_xTe$ at low temperature regions, however with increasing temperature, Power factor of SnTe is increased gradually, besides SnTe has a better power factor than all samples at 673K. Although the samples have high electrical conductivity due to mixed two phases, Samples has lower power factor due to the low Seebeck coefficient.

Chapter 5. Conclusion

(1) We developed the measurement of the thermoelectric power in the temperature range from 2K to 300K. Our equipment is composed of two heaters, two thermometer, chip resistors, etc. Supplied heat by current source is provided temperature difference between two thermometers. Temperature difference serves voltage difference by carriers of sample and the difference is measured by voltmeter. By this time the Seebeck coefficient is calculated by voltage and temperature difference. In addition, high density data is obtained by two heaters that are operated by turn. The system is controlled by LabVIEW software. In order to demonstrate this system, the results of Pt wire match with reference data besides. The Seebeck coefficient is zero in superconducting state, so we used $Ca_{10}Na_x(Pt_3As_8)(Fe_2As_2)_5$ as superconductor. As a result, the estimated uncertainty of this system from 77K to300 K temperature ranges falls within a maximum of $\pm 1\ \mu V\ K^{-1}$. Superconducting transition temperature of $Ca_{10}Na_x(Pt_3As_8)(Fe_2As_2)_5$ is about 37K, besides, the Seebeck coefficient is zero below 37K in $Ca_{10}Na_x(Pt_3As_8)(Fe_2As_2)_5$. Thus, the equipment is calculated by Seebeck coefficient of superconductor and Pt wire. In conclusion, we demonstrated the equipment with superior performance through confirming calculated data.

(2) Before hot pressing and after, XRD patterns of $Sn_{1-x}Ag_xTe$ are changed from two phases to mixed phase. Here, after hot pressing, we noticed that mixed phase is more dominant than Ag-doping effect because Ag ionic radius and atomic radius is larger than ionic radius of Sn. In addition, lattice parameter of mixed SnTe/AgTe is between lattice parameter of SnTe and AgTe. By XRD analysis, we have confirmed that the samples are

composed of mixed SnTe and AgTe. Ultimately, lattice parameter of AgTe expanded and SnTe is decreased by mixed SnTe and AgTe.

Through electrical conductivity of the samples, we could confirm that electrical conductivity of the samples is well-maintained until high temperature. For this reason, we can suggest that the samples become more metallic than SnTe due to mixed phase (SnTe/AgTe) at grain boundary.

Then, the Seebeck coefficient of the samples was decreased with increasing Ag-concentration. Besides, the Seebeck coefficient of sample to include silver(x=0.1) is approximately 55 μV/K. However, excluding low temperature region, the Seebeck coefficient has lower value than SnTe. Similar to tendency of the Seebeck coefficient, the power factors, which is calculated from Seebeck coefficient and electrical conductivity, is decreased with increasing Ag-concentration. The power factor of sample to include silver(x=0.1) has maximum value (1.1 mW/mK^2) at 673K. However, SnTe has higher power factor than Ag-included SnTe.

Nevertheless, by mixed two phases, high electrical conductivity of the samples is kept until high temperature. Thus, we can carefully expect that sample to include mixed phase obtain high electrical conductivity.

References

[1] A V shevelkov, Russian Chemical Rivews 77 (1) 1-19 (2008).

[2] J. R. Stootsman, D. Y. Chung, and M. G. Kanatzidis, Angew. Chem. Int. Ed. 48, 8616-8639 (2009).

[3] Lon E. bell, Science 321, 1457 (2008).

[4] Xin Liang, "Structure and Thermoelectric Properties of ZnO Based Materials" ph.D. Thesis, Harvard University, Cambridge, Massachusetts, 227pages. (2013)

[5] Biswas, K.; He, J.; Blum, I. D.; Wu, C. I.; Hogan, T. P.; Seidman, D. N.; Dravid, V. P.; Kanatzidis, M. G. Nature 489, 414. (2012)

[6] Zhao, L. D.; He, J.; Hao, S.; Wu, C. I.; Hogan, T. P.; Wolverton, C.; Dravid, V. P.; Kanatzidis, M. G. J. Am. Chem. Soc. 134, 16327. (2012)

[7] Brebrick RF, Strauss AJ Anomalous thermoelectric power as evidence for two valence bands in SnTe. Phys Rev 131(1):104–110. (1963)

[8] Efimova BA, Kaidanov VI, Moizhes BY, Chernik IA Band model of SnTe. Sov Phys-Sol Stat 7(8):2032–2034. (1966)

[9] Rogers LM Valence band structure of SnTe. J Phys D Appl Phys 1(7):845–848. (1968)

[10] Santhanam S, Chaudhuri AK Transport-properties of SnTe interpreted by means of a 2 valence band model. Mater Res Bull 16(8):911–917. (1981)

[11] Singh DJ Thermopower of SnTe from Boltzmann transport calculations. Funct Mater Lett 3(4):223–226. (2010)

[12] Brebrick, R. F. J. Phys. Chem. Solids 24, 27. (1963)

[13] Kafalas, J. A.; Brebrick, R. F.; Strauss, A. J. Appl. Phys. Lett., 4, 93. (1964)

[14] Zhang Q, et al. Heavy doping and band engineering by potassium to improve the thermoelectric figure of merit in p-type PbTe, PbSe, and PbTe(1-y)Se(y). J Am Chem Soc 134(24):10031–10038. (2012)

[15] Q. Zhang, B. L. Liao, Y. C. Lan, K. Lukas, W. S. Liu, K. Esfarjani, C. Opeil, D. Broido, G. Chen and Z. F. Ren, Proc. Natl. Acad. Sci. U. S. A., 110, 13261–13266. (2013)

[16] G. Tan, L.-D. Zhao, F. Shi, J. W. Doak, S.-H. Lo, H. Sun, C. Wolverton, V. P. Dravid, C. Uher and M. G. Kanatzidis, J. Am. Chem. Soc., 7006–7017. (2014)

[17] Changhoon Lee, Jisook Hong, Myung-Hwan Whangbo, and Ji Hoon Shim, Chem. Mater. 25, 3745−3752 (2013)

[18] M. cutiler, J. K. Leavy, R. L. Fitzpatrick, Phys. Rev. 133, A1143 (1964)

[19] N. F. Mott, H. Jones, 'The theory of the properties of metals and alloys', Dover, New York (1958)

[20] E. Moon, S. L. Bud'ko, M. S torikachvili, P. C Canfield Meas. Sci. Technol. 21, 055104 (2010)

[21] D. M. Freik, A. G. Mikolaichuk, B. F. Bilenkii, physica status solid, 28, 0 (1968)

[22] Popova et al., Ookl. Chem. Technol. 201, 155 (1971)

[23] Min Zhou, Zachary M. Gibbs, Heng Wang, Yemao Han, Caini Xin, Laifeng Li, and G. Jeffrey Snyder. Phys. Chem. Chem. Phys., 16,20741 (2014)

요 약 문

열전 성능이 우수한 Pb-based 물질은 환경적으로 독성을 가진다. 따라서 Pb-based 물질은 독성이 없는 물질로 대체 되어야 한다.

Tin telluride (SnTe) 는 PbTe, PbSe 와 같은 rock salt 구조 이다. 게다가 SnTe 는 PbTe, PbSe 의 전자 밴드 구조 (두 개 밴드 구조)와 유사한 밴드구조를 가졌다. 따라서 작은 제백상수와 큰 열전도도를 극복한 SnTe 좋은 열전재료가 될 것으로 기대된다. 그래서 실버가 포함된 poly crystals 이 박스 퍼니스와 핫프레스에 의해 준비되었다. 우연적으로 우리는 $Sn_{1-x}Ag_xTe$ 의 XRD 패턴이 핫프레스 전후에 바뀌는 것을 알았다. 그리고 핫프레스 전에는 두개의 사에서 후에는 섞인 패턴이 발견 되었다. 게다가 섞인 패턴 때문에 샘플들의 전기전도도는 높은 온도까지 잘 유지했다. 파워팩터는 실버(x=1)에서 가장 높은 값 (1.1 mW/mK^2) 을 673K 에서 가졌다. 그러나 parent SnTe 는 실버가 포함된 시료보다 높은 파워팩터를 가졌다. 그럼에도 불구하고, 우리는 샘플이 상이 섞인 상태에서 높은 전기전도도를 가진다고 조심스럽게 예측 해볼 수 있다.

예외적으로 우리는 2K-300K 까지 측정할 수 있는 열전측정 장비를 개발했다. 장비는 두 개의 히터, 두 개 온도계, 칩 저항, 등으로 이루어져있다. 게다가 두 개의 히터가 번갈아 가면서 작동하기 때문에 높은 밀도의 데이터를 얻을 수 있다. 이 시스템은 랩뷰 소프트웨어에 의해 조작된다. 측정 장비를 증명하기 위해 우리는 Pt wire 의 참고 데이터와 실험과 비교하였고, 초전도체인 $Ca_{10}Na_x(Pt_3As_8)(Fe_2As_2)_5$ 으로 비교함으로써 우수한 성능을 확인하였다.

핵심어: SnTe, 섞인 상태, 전기전도도, 제백상수, 파워팩터